Food Chemistry 443 (2024) 138579

Contents lists available at ScienceDirect

Food Chemistry

journal homepage: www.elsevier.com/locate/foodchem

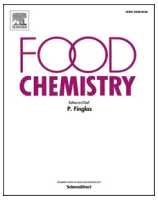

Multilayer microparticles for programmed sequential release of phenolic compounds from *Eugenia stipitata*: Stability and bioavailability

Williara Queiroz de Oliveira [a,*], Iramaia Angélica Neri Numa [a], Izabela D. Alvim [b], Henriette M. C. Azeredo [c], Leticia B. Santos [c,d], Felipe T. Borsoi [a], Fábio F. de Araújo [a,e], Alexandra C.H.F. Sawaya [e], Gustavo C. do Nascimento [f], Maria Teresa P.S. Clerici [f], Célio K. do Sacramento [g], Glaucia Maria Pastore [a]

[a] *Laboratory of Bioflavours and Bioactive Compounds, Department of Food Science, Faculty of Food Engineering, University of Campinas, 13083-862 Campinas, SP, Brazil*
[b] *Technology Center of Cereal and Chocolate, Food Technology Institute (ITAL), 13070-178 Campinas, SP, Brazil*
[c] *Embrapa Instrumentation, R. 15 de Novembro, 1452, 13560-970 São Carlos, SP, Brazil*
[d] *Graduate Program in Food, Nutrition and Food Engineering, UNESP – São Paulo State University, Rodovia Araraquara-Jaú, km 01, 14800-903 Araraquara, SP, Brazil*
[e] *Faculty of Pharmaceutical Science, University of Campinas, 13083-871 Campinas, SP, Brazil*
[f] *Department of Food Science and Nutrition, School of Food Engineering, University of Campinas, 13083-862 Campinas, SP, Brazil*
[g] *Department of Agricultural and Environmental Sciences, State University of Santa Cruz, 45662-900 BA, Brazil*

ARTICLE INFO

Keywords:
Araçá-boi
Cará-roxo
Co-encapsulation
In vitro digestion
Spray drying
Spray chilling

ABSTRACT

A co-delivery system based on multilayer microparticles was developed and characterized for the sequential release of phenolic compounds (PCs) using different encapsulation processes (spray drying: SD and drying-chilling spray: SDC) and wall materials to improve the stability and bioavailability of PCs. Samples were characterized in terms of process yield (PY%), phenolic retention efficiency (PRE%), chemical structure and crystallinity (NMR, FTIR, DXR), thermal stability (DSC and FT-IR), anti-radical capacity (ORAC and ABTS) and *in vitro* digestion. PRE% of samples by SD were higher ($p < 0.05$) than SDC due to the formation of PCs from CRF (cará-roxo flour). NMR, FTIR, DXR confirmed the presence of key components and interactions for the formation of the advanced co-delivery system. The SDC particles showed crystalline regions by XRD and were stable at ~47 °C. All samples showed good release of PC in the intestinal phase, and antiradical capacity that reached 23.66 μmol TE g^{-1}.

1. Introduction

The consumption of fruits and vegetables is widely discussed as promoting the reduction of chronic diseases. In Brazil, there is a wide variety of fruits from tropical and subtropical regions. The araçá-boi (*Eugenia stipitata*) is a native plant of the Amazon basin and rich in volatile terpenes, fiber, vitamin C, carbohydrates (65 to 72% w/w), proteins (8 to 10% w/w), compounds phenolics (PC), in addition to presenting antioxidant properties, antimutagenic and anti-inflammatory activities (de Araújo et al., 2019).

Our previous studies have demonstrated that a PC-rich diet can promote redox homeostasis, block the generation of ROS/RNS, and stop the propagation of reactive species through the chelation of metal ions (de Oliveira et al., 2021b). However, despite the benefits mentioned, PCs are unstable and can be affected by external physicochemical factors such as oxygen, light, heat, and humidity, in addition to restricted bioaccessibility and bioavailability (Lopez-Polo et al., 2020).

PC encapsulation is considered a viable option to improve technological, nutritional and sensory properties (Oliveira et al., 2020). Several studies have already reported encapsulation systems for phenolic compounds using various techniques, such as emulsions, liposomes, electrospray, inclusion complexes, ionic gelation, drying and chilling spray (Hatefi & Farhadian, 2020; Human et al., 2019; Lopez-Polo et al., 2020; Mehran et al., 2020; Rezaei et al., 2020). However, few studies have designed multilayer microparticle systems for phenolic release using combined encapsulation, *e.g.*, spray drying (SD) followed by spray

* Corresponding author at: Laboratory of Bioflavours and Bioactive Compounds, Department of Food Science, Faculty of Food Engineering, University of Campinas, Monteiro Lobato Street, 80, 13083-862 Campinas, São Paulo, Brazil.
E-mail address: w229276@dac.unicamp.br (W. Queiroz de Oliveira).

https://doi.org/10.1016/j.foodchem.2024.138579
Received 16 October 2023; Received in revised form 7 January 2024; Accepted 23 January 2024
Available online 26 January 2024

chilling (SDC).

SD is widely used to retain bioactives within the wall material. Furthermore, the technique has high efficiency and low cost (Mehran et al., 2020). SD microparticles result in powder with low water activity (a_w), which simplifies handling, storage and transportation, also guaranteeing microbiological quality (de Oliveira et al., 2021b). Conversely, spray chilling encapsulation (SC), also known as and with synonyms such as spray chilling, spray congealing or prilling or cooling, can improve the functionality, solubility, and protection of bioactives, in addition to achieving a controlled release profile in the small intestine (de Oliveira et al., 2021a; Favaro-Trindade et al., 2021).

When it comes to microparticle structuring and PC entrapment, there is a growing demand for new sources of hydrocolloids (Hernández-Barrueta et al., 2020). In this context, plant polysaccharides continue to be studied as an effective component for the formulation of encapsulating matrices as they are GRAS, sustainable, profitable and have pro-health activity (Goksen et al., 2023). Cará-roxo (*Dioscorea trifida*) is an Amazonian tuber of high nutritional quality, being considered a promising source of antioxidants (Teixeira et al., 2016); anti-inflammatory (Mollica et al., 2013); antihyperlipidemic and antidiabetic properties; in addition to being considered one of the most economically important tubers for the Amazon region (Teixeira et al., 2016).

For the first time, a blend of purple cará-roxo (CRF) and gum arabic (GA) was used for wall structuring (CRF-GA) by SD, containing araçá-boi extract (ABE) as core material, followed by encapsulation by SC, using vegetable fat (VF) and hydrogenated palm oil (HPO) to form multilayer microparticles (SDC). The objective of this work was to develop and characterize an advanced co-delivery system based on multilayer microparticles for the programmed sequential release of phenolic compounds (PCs), using different encapsulation processes (SD and SC) and wall materials (CRF-GA and FV-HPO) to improve the stability and bioavailability of PCs. To this end, several aspects of encapsulation were studied, including analysis of chemical structure, thermal stability, antiradical capacity, and *in vitro* digestion.

2. Materials and methods

2.1. Materials

Ripe araçá-boi fruits were collected in Ituberá, BA, Brazil (geographic coordinates 13°44″ S 39°9″ W). The botanical identification (n° 55.875) was deposited in the Herbarium-UEC of the Agronomic Institute of Campinas, SP, Brazil. The CRF was kindly provided by the Laboratory of Cereals, Roots, and Tubers of the College of Food Engineering (FEA-Unicamp), Campinas, SP, Brazil. Arabic gum (GA, InstantGum AA, Nexira, São Paulo, SP, Brazil) was obtained at the Chocotec Cereals Laboratory, Food Technology Institute (ITAL), Campinas, SP, Brazil. Phenolic standards were purchased from Sigma-Merck (Darmstadt, Germany) and Fluka Chemical Co. (Milwaukee, WI, USA). Ethanol (Dinâmica, SP, Brazil), methanol (Sigma-Merck, Darmstadt, Germany) and toluene (Synth, SP, Brazil) were of analytical grade.

2.2. Extraction of ABE

After collection and cleaning, the edible parts of the araçá-boi (pulp and peel) were processed followed by the green extraction of phenolic compounds, according to Araújo et al. (2021). Then 10 g of lyophilized powder of araçá-boi were solubilized in 150 mL of hydroethanolic solution (8:2 v/v). After that, they were sonicated (10 min/25 °C) (Ultrasonic Cleaner, model SSBu, São Paulo, Brazil) and centrifuged (4000 g, 5 min, 5 °C) (Rotanta, 460 R, Tuttlingen, Germany). After collecting the supernatants, the residues were washed twice more under the same conditions. Subsequently, supernatants were exhaustively rotary evaporated (40 °C) (RII Evaporator model, Flawil, Switzerland). The final volume of araçá-boi extract (ABE) was adjusted to 50 mL of water and stored under refrigeration (-20 °C) until use.

2.3. Preparation of multilayered structural microparticles

2.3.1. Encapsulation of phenolics by spray drying (SD)

The SD microparticles, with solid concentration fixed at 50 g for 250 g of liquid, were named SDT3 (CRF: 9.94 g, ABE: 0.29 g, GA: 39.25 g) and SDT4 (CRF: 9.94 g, ABE: 0.44 g, GA: 39.13 g). The starting materials were homogenized (4.000 g 10 min^{-1}) (Ultra Turrax®, T18, IKA, Staufen Germany). SDT3 and SDT4 were produced with a mini-spray dryer (B-290, Buchi, Flawil, Switzerland), using the same operating parameters reported by Fadini et al., (2018) (**Supplementary material 1**).

2.3.2. Co-encapsulation of phenolic microparticles by spray chilling (SC)

SDT3/T4 by SD were co-encapsulated by spray chilling (SC) resulting in double-layer microparticles, which were named SDCT3 and SDCT4. To this end, the process was adapted in a mini spray dryer connected to a B296 dehumidifier (Büchi, Flawil, Switzerland) to produce cold, as adapted from Alvim et al. (2016) (**Supplementary material 1**). The second wall layer was composed of a mixture of vegetable fat (VF), hydrogenated palm oil (HPO), polyglycerol polyricinoleate (PGPR) emulsifier. SDCT3 and SDCT4 presented a ratio of 1: 2: 2: 0.2, of microparticles (SDT3 or SDT4), FV, HPO, PGPR, respectively, having a softening point of 52.05 ± 0.11 °C and crystals of the type β (Fadini et al., 2018).

2.4. Encapsulation index

Process yield (PY). PY (%) (**Eq. (1)** was calculated as the ratio between the mass of solids at the end of the process (m_f) and the initial total mass (m_i) used in the preparation of the microparticles, according to Oliveira et al. (2020).

$$PY\,(\%) = \frac{m_f}{m_i} \times 100 \quad (1)$$

Phenolic retention efficiency (PRE). To determine PRE (%), 50 mg of microparticles were dispersed in Milli-Q water (1 mL), vortexed (1 min) (PHOX, model MS-S2, Paraná, Brazil) and sonicated (10 min) (Ultrasonic Cleaner, model SSBu, São Paulo, Brazil). Subsequently, they were centrifuged at 4000 g (5 min, 5 °C), filtered (0.22 um) and injected into UHPLC-ESI-MS (Acquity UPLC–TQD, Waters, Milford, USA). Ten phenolic compounds found in preliminary investigation, namely quercetin, rutin, myricetin, kaempferol, chlorogenic, protocatechuic, cinnamic acid, ferrulic, p-coumaric, and *trans*-cinnamic acid were used as a chemical marker to determine the retention efficiency of phenolic compounds (PRE). The PRE was determined as the percentage of the final content (C_f) in the microparticles of each PC in relation to the initial content (C_i) (**Eq. (2)** (Silva Faria et al., 2020).

$$PRE\,(\%) = \frac{C_f}{C_i} \times 100 \quad (2)$$

2.5. Structure characterization

2.5.1. Scanning electron microscopy (SEM) and particle size

The morphology of the microparticles was observed by scanning electron microscopy (SEM) (JSM 6510, Jeol, Tokyo, Japan), according to Oliveira et al. (2020). The microparticles were coated with a layer of gold (10 nm) by sputtering (ACE600, Sputter Coater, Leica Microsystems, Wetzlar, Germany), using a current of 40 mA 60 s^{-1}. Samples were examined using an accelerating voltage of 5 kV and a working distance of 10 mm, with magnification ranging from 40 to 2200×. The mean diameter and particle size distributions were determined by laser diffraction using the wet method (LV950-V2, Horiba, Kyoto, Japan) with dispersion in 99.5% ethanol, according to Paulo et al. (2022).

2.5.2. Carbon-13 CP/MAS NMR

The structure of the samples was analyzed by ^{13}C nuclear magnetic resonance (NMR) in the solid state, with cross polarization (CP) and rotation around the magic angle (MAS) in a Bruker AVANCE III HD 400 (Bruker, Germany), according to Karaaslan et al. (2021). The samples were placed in a 4 mm zirconia rotor and rotated at 10 kHz.

2.5.3. FTIR analysis of microparticles

Infrared absorption spectra were performed on an Fourier Transform Infrared Spectroscopy (FTIR), model Vertex 70 (Bruker, Germany) spectrophotometer, equipped with an attenuated total reflectance (ATR) mode, in the range of 400 to 4000 cm $^{-1}$, resolution of 4 cm $^{-1}$ and 32 accumulations, according to Pereira de Oliveira et al. (2022).

2.5.4. X-Ray diffraction (XRD) measurements

XRD was performed using the XRD-6000 diffractometer (Shimadzu, Kyoto, Japan). The samples were submitted to direct analysis, using Cu Kα radiation, (λ = 1.540560 Å) (Niyom et al., 2019). 2θ ranged from 5° to 60°, with a sweep speed of 0.1° s^{-1}. The degree of crystallinity (Xc) of the microparticles was then calculated via **Eq.3**.

$$Xc = \frac{R_c}{R_c + R_a} \times 100 \quad (3)$$

where *Xc* represents the degree of crystallinity, *Rc* represents the crystalline regions, and *Ra* represents the amorphous regions.

2.6. Thermal analysis

Differential scanning calorimetry (DSC). The thermal analysis of the samples was performed by DSC (Bajac et al., 2022). 2–5 mg of the samples were hermetically sealed in an aluminum pan, and the scanning was performed at 10 °C min^{-1} in a temperature range between 10 °C and 200 °C, with an ultrapure nitrogen flow rate of 50 mL min^{-1}. The glass transition temperature (*Tg*) was taken as the inflection point of the thermal curve, caused by the discontinuity of the specific heat (Iturri et al., 2021).

Thermogravimetric Analysis (TGA). TGA was performed in a TA Instruments thermobalance (Q500, New Castle, USA) at a temperature range of 30–600 °C, in a platinum crucible with approximately 3 g of sample, under a dynamic nitrogen atmosphere (50 mL min^{-1}), and heating rate of 10 °C min^{-1} (Machado et al., 2022).

2.7. Simulation of the gastro-intestinal digestion

Gastric digestion. Simulated Gastric Fluid (SGF) and Simulated Intestinal Fluid (SIF) electrolyte solutions were prepared (de Araújo et al., 2021b). 1 mL of each phenolic extract was homogenized in 3.5 mL of saline solution (140 mmol L $^{-1}$ NaCl, 5 mmol L $^{-1}$ KCl), and the pH of the mixture was adjusted to 2.0 with 6 mol L $^{-1}$ HCl. 125 μL of swine pepsin solution (Sigma-Aldrich, 200 mg of 424 U mg $^{-1}$ pepsin in 5 mL of 0.1 mol L $^{-1}$ HCl) were added and the samples were incubated in a water bath, with agitation at 130 rpm for 1 h at 37 °C. 2 mL of chyme were collected and stored in a freezer at −80 °C for subsequent analysis.

Intestinal digestion. After the gastric digestion steps, the digesta pH was adjusted to 6.8 by adding 1 mol L $^{-1}$ $NaHCO_3$. Then, 625 μL of pancreatin and bile solution (Sigma-Aldrich, 225 mg of bile extract and 37 mg of pancreatin with activity equivalent to 4x U.S.P, diluted in 18.7 mL of 0.1 mol L $^{-1}$ $NaHCO_3$) were added and the samples were incubated at 37 °C and 130 rpm for 2 h. At the end of the intestinal phase, the samples were cooled in an ice bath and the digested volume adjusted to 5.5 mL with saline solution and stored at −80 °C until the moment of analysis.

Fractions were ultrafiltered (4000 g/30 min/5 °C) (Rotanta, 460 R, Tuttlingen, Germany) using Amicon Ultra centrifugal filtration devices (30 kDa, Millipore). A sample of saline solution at pH 7.0 (blank) was also subjected to all digestion procedures to eliminate reagent interference.

2.8. In vitro antioxidant activity assays

2.8.1. Oxygen radical absorbance capacity (ORAC)

ORAC was determined according to Neri-Numa et al. (2020). Trolox curve concentrations (25, 50, 100, 200, 300, 400, 500, 600 μM) were prepared in phosphate buffer (PBS) (pH 7.4, 75 mM). The samples, dissolved in PBS, had concentrations of 10 mg mL^{-1}. The samples (20 μL) and the fluorescein solution (120 μL; 70 μM, which was the final concentration) were mixed in one of the 96 wells of a black microplate. Then, 60 μL of an AAPH solution (final concentration of 12 mM) was added and the fluorescence was checked (60 s/80 cycles) in a microplate reader (NOVOstar®, model BMG Labtech, Offenburg, Germany), with fluorescence filters (excitation: λ 485 nm; emission: λ 520 nm). The experiment was conducted at 37 °C, under conditions of pH 7.4 and with a blank sample in parallel. Results were expressed as equivalents for μmol TE g^{-1} of PRP.

2.8.2. $ABTS^+$ scavenging capacity assay

The ABTS+ clearance assay was determined based on the method described by Araújo et al. (2021a). The ABTS radical was generated from the reaction of 5 mL ABTS (7 mmol) with 88 μL of potassium persulfate (140 mmol). The solution was kept at rest (16 h, 25 °C) and, after that, had its absorbance adjusted to 0.70 ± 0.02 at 734 nm in a microplate reader (SpectrostarNano, BMG Labtech, Germany). For reading, 50 μL of sample and 250 μL of ABTS+ solution was injected at 734 nm. Trolox was used to create the analytical curve (5–150 μM mL $^{-1}$) and the results were expressed in μmol TE g $^{-1}$ PRP.

2.9. Detection of phenolic compounds with UPLC-ESI-QTOF-MS

The characterization of the phenolic compounds present in the samples was performed according Fernandes de Araújo et al. (2020). 50 mg of the samples were dissolved in 1.0 mL Milli-Q water. Each solution was injected into an ultra-high performance chromatography mass spectrometry system (Acquity UPLC–TQD, Waters, Milford, USA) with an Acquity UPLC BEH C18 column of 1.7 μm microparticles (2.1 × 50 mm) and an oven temperature of 30 °C. A gradient with a flow rate of 0.20 mL min-1 and injection of 10 μL was used, consisting of solvent A (0.1% formic acid in Milli-Q water) and solvent B (acetonitrile). The conditions were as follows: starting with 98% A and 5% B and increasing to 100% B in 8 min, which was maintained for 9 min. In 9.1 min it returned to the initial conditions, stabilizing the system up to 10.00 min. The mass spectra, with electrospray ionization (negative mode), were acquired under the following conditions: (i) capillary and cone voltages of –3.5 kV and − 30 V, respectively, source temperature 150 °C and temperature of desolvation of 350 °C. Ions, in SIM mode, were acquired in the range *m/z* 100–700.

The phenolic compounds (PC) present in the samples were identified by comparing their UPLC-ESI-QTOF-MS dissociation patterns and retention time with the standards. PC amounts were determined by comparison with the standard calibration curve. Stock solutions of each standard compound (1 mg mL $^{-1}$) were prepared in methanol and stored. Dilutions of stock solutions were made at 9 different levels for calibration curves of 0.005; 0.01; 0.05; 0.1; 0.5; 1; 5; 10; 50 μg mL^{-1} of standard compounds, with results expressed in the same unit (μg mL^{-1}).

2.10. Statistical analysis

Data were evaluated using analysis of variance (ANOVA) and Tukey tests in MINITAB (version 13.2, MINITAB Inc. 2000). All experiments were repeated three times and significance was set at $p < 0.05$.

3. Results and discussion

3.1. Encapsulation indexes

PY (%) and PRE (%) depend on the characteristics of the polymers, the affinity of the bioactive compounds with the wall material and the parameters of the encapsulation process (Comunian et al., 2016). Although the PRE% did not reveal significant differences ($p < 0.05$) between the encapsulation processes (SD or SDC), the microparticles generated by the SDC method (42.16% ± 4.55[a]) exhibited a process yield (PY%) higher compared to the SD method (34.72% ± 0.03[a]). This can be attributed to the more rigorous conditions during the SD process that involve exposure to high temperatures and turbulence, which can result in losses in the equipment's piping and chambers (de Oliveira et al., 2021b; Iturri et al., 2021). In contrast, SC is a milder process, with less particle breakdown and less loss of volatile compounds (Premjit et al., 2022). Our SD results were superior to those of Tzatsi & Goula (2021) (8.12–31.93%) when encapsulating chokeberry extract and superior pectin microparticles produced by SD (36.29%) (Li et al., 2022). Previous studies showed that SC encapsulation was similar to the yield found in our studies (43.02%) when encapsulating pigment-polyethylene glycol (Banožić et al., 2022).

The PRE (%) of phenolic compounds are shown in **Supplementary Material 2**. The highest PRE values (%) were found in SDT3/SDT4, referring to protocatechuic, *trans*-cinnamic and ferulic acids, higher than previously reported (Badawi et al., 2022). Minimal PRE (%) were found for myricetin, quercetin and rutin, not reaching 2%, which indicates intense degradation. SDSCT3/T4 showed greater retention for ferulic, protocatechuic and p-coumaric acids, with PC retention values similar to Cutrim et al. (2019). A tendency towards higher PRE (%) in microparticles per SD was observed, with values above 100% for protocatechuic, *trans*-cinnamic and ferulic acids, mainly in SDT4. This behavior may be associated with a greater detachment of PC from the food matrix when subjected to heat (150 °C) during the SD process, especially in a whole product, such as CRF. Despite the fact that synthesis of phenolic compounds is a less common process than degradation, heat can make the cell wall permeable, increasing the solubility and diffusion of PCs (Antony & Farid, 2022). Furthermore, heat can break down complex structures, such as polymerized phenolics or those linked to sugars and proteins (Angelo & Jorge, 2007). Antony & Farid (2022) reported that lignin can be degraded at high temperatures, giving rise to phenolic acids. The same authors cited a significant increase in total phenolic content at 150 °C (Antony & Farid, 2022). Other studies have also correlated an increase in temperature (180–200 °C) with an increase in PC content and antioxidant activity (Andrew et al., 2020). This highlights the complexity of the interactions between the PC and encapsulation processes, which, in addition to promoting stability (Neuenfeldt et al., 2022), also demonstrate an increase in nutritional quality of the microparticles in this study.

3.2. Morphology and particle size

Particle size influences the bioavailability and bioaccessibility of phenolic compounds released from controlled release systems with multilayer microparticles (Bajac et al., 2022; Oliveira et al., 2022). D50 of SDC particles (SDCT3: 64.33 ± 2.20[b] and SDCT4: 76.84 ± 7.15[a] μm) was higher ($p < 0.05$) than those of the SD sample (SDT3:15.72 ± 0.25[c] and SDT4: 14.23 ± 0.18[c] μm). Alvim et al. (2016) and Santos et al. (2023) observed that spray chilling microparticles are significantly larger than spray dry microparticles because, in SD, the droplets contract due to solvent evaporation, whereas, in SD, the droplets solidify in a cold lipophilic medium, preventing changes in droplet size throughout the process. However, our microparticles are suitable for food application because their D50 diameters are between 14 and 76.80 μm. Diameters smaller than 100 μm do not affect the texture and are not noticeable by the consumer (Oliveira et al., 2020). Previous studies using combined encapsulation of SDC to protect carotenoids and polyunsaturated fatty acids (PUFAs) obtained microparticles with D50 of 96 and 81.31 μm, respectively, larger than our findings (Pinho et al., 2022). A bimodal distribution was observed in the multilayer microparticles, with polydispersity index (span) ranging from 5.60 to 5.80. The greater the amplitude value, the less homogeneity of sizes within a particulate system. However, the presence of a bimodal distribution may allow sequential or controlled release of different compounds. Similar span value (5.0) was found in double shell microparticles (SDC) containing fish oil (Fadini et al., 2019).

SEM is essential to understand the release of phenolics in multilayer microparticles and to evaluate the integrity and morphology of the microparticles (Bera et al., 2021). The morphology of the microparticles is shown in Fig. 1**.** SDT3/T4 were semi-spherical, wrinkled, irregular and with an evident presence of dents on the surface, due to rapid evaporation during spray drying, however, with good integrity, without fractures, cracks or any other defects (Bajac et al., 2022; Mahdi et al., 2020b; Porras-Saavedra et al., 2021). Particle surface irregularity can be useful, contributing to better dispersibility and rehydration (Bajac et al., 2022). In contrast, SDCT3/T4 (Fig. 1 **c, d**) presented spherical shapes and smooth surfaces, resulting from the controlled solidification of the matrix, which prevents the formation of rough or textured structures, which was already expected since there is no mass transfer process or forces and gradients that can distort the structure (Santos et al., 2023). Having a spherical appearance is interesting for industrial applications, by increasing fluidity in pipes. However, the irregularity of surface microparticles can be useful, contributing to better dispersibility and rehydration (Bajac et al., 2022; Santos et al., 2023). SEM analysis results were in line with previous studies (Aguiar et al., 2023; Bajac et al., 2022; Porras-Saavedra et al., 2021).

3.3. Carbon-13 CP/MAS NMR and FTIR analysis

The chemical structure of SD and SDC microparticles was characterized by CP/MAS Carbon-13 NMR spectroscopy. Fig. 2**a** shows chemical changes and characteristic peaks. Samples SDT3/T4 exhibited similar NMR patterns, with resonance peaks seen at 63, 75, 80, 100 and 175 ppm. The deviation of 63 ppm can be attributed to the presence of arabinan (C5), and the high intensity deviation at 72 ppm can be associated with the galactan (*C*2) of GA, indicating that the gum is the most important component from a structural point of view, being responsible for the formation of a three-dimensional network that held the microparticles together (Isobe et al., 2020). C3 of arabinan had a calculated displacement of 82 ppm (Isobe et al., 2020; Ndiwe et al., 2019; Sabet et al., 2021). Changes between 72 and 82 ppm are typical of the carbohydrate region (the central peak of sugars), with considerable width indicating carbohydrate oligomers from GA (D-galactose, L-arabinose, L-rhamnose) and CRF (Ndiwe et al., 2019). The 100–104 ppm range can be assigned to anomeric C1 carbons (Sabet et al., 2021). SDT3 and SDT4 showed peaks that could be carboxy groups of galacturonic acid at 175 ppm in salt form (-COOX; X: cation) (Isobe et al., 2020). These results provide evidence that SDT3/T4 have a chemical structure that is favorable to encapsulation and had arabinan, galactan, and galacturonic acid as major components (Funami et al., 2011).

SDCT3/T4 (Fig. 2**a**) exhibited similar resonance profiles, with peaks at 14, 25, 33, 65, 70 and 175 ppm. The peak of 14–25 ppm are associated with protons bound to methyl groups (–CH3) present in oleic acid (C18:1) (C1), linoleic acid (C18:2) (*C*2) and α-linolenic acid (C18: 3) (C3) from HPO, and only the peak of 14 ppm is due to cis fatty acids (Di Pietro et al., 2020; Truzzi et al., 2021). The peak at 33 ppm can be attributed to the resonance of carbons close to the carboxyl radical (–CH2COOH-) (*C*2), while the peak at 65 ppm can be associated with glycerol carbons (C1/C3 and *C*2), mainly from FV. Furthermore, a peak was observed at 175 ppm, attributed to the presence of palmitic acid in C1 of the triacylglycerols (Di Pietro et al., 2020; Truzzi et al., 2021). These results indicate that the SDC encapsulation was successful and

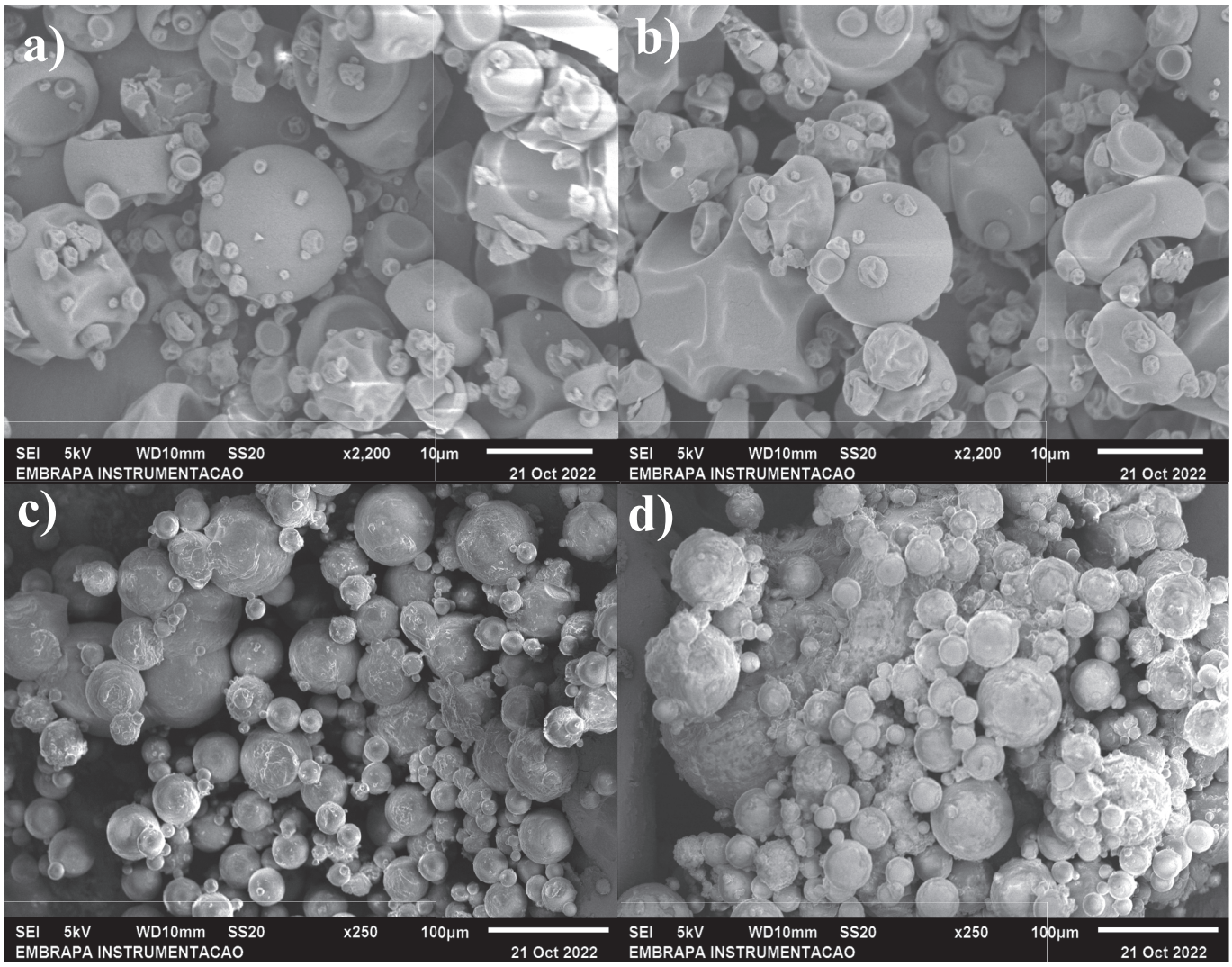

Fig. 1. SEM micrographs of spray drying particles a) SDT3, b) SDT4 and spray chilling multilayer particles c) SDSCT3 and d) SDSCT4. SDT3 (CRF: 9.94g, ABE: 0.29g, AG: 39.25g), SDT4 (CRF: 9.94g, ABE: 0.44g, AG: 39.13g), and (SDCT3/T4), composed of a mixture of vegetable fat (FV), hydrogenated palm oil (HPO) and particles (SDT3 or SDT4), and 4.0 g o f polyglycerol polyricinoleate (PGPR), in a ratio of 1:2:2:0.2. ABE (*araçá-boi* extract), CRF (*cará-roxo* flour), and GA (gum arabic).

modified the structure of SDT3/T4, forming a lipid matrix around the original constituents, important to improve the stability and functional properties of the microparticles.

The FTIR spectra are shown in Fig. 2**b**. Most of the bands are common in polysaccharides and polysaccharide-containing materials, although some shifts and/or changes in intensity are noticeable. The broad band at 3310 cm^{-1} is attributed to OH elongation (Rizkyana et al., 2022). All spectra have a band around 2920 cm^{-1}, due to CH stretching, but samples SDCT3/T4 show two especially intense bands in this region, due to the superposition of asymmetric stretching vibrations of CH or CH2 derived from the presence of lipids in the samples by SC (Rizkyana et al., 2022). Other bands that were intensified by the presence of lipids in these microparticles are the one at 1737 cm^{-1}, attributed to C═O stretching, and the one at 1463 cm^{-1} due to C—H bending (Dong et al., 2014). The band at 1172 cm^{-1} is also found in spray chilling samples, due to the asymmetric elongation vibration of O—C—C bonds (Martínez et al., 2018). Evaluating the differences between the spectra of the starting materials and the microparticles, it was possible to observe some significant changes. For example, the 1641 cm^{-1} band almost disappeared in the encapsulated samples due to the O—H bending vibration of water in CFR and ABE, indicating the reduction in the amount of free water after SD, which has positive applications for stability (Asranudin et al., 2021). Some bands almost disappeared in the spray chilling samples, like the one at 1602 cm^{-1} attributed to asymmetric COO– stretching in GA (Amirabadi et al., 2020), the one at 1147 cm^{-1} corresponding to the symmetric stretching of C—O—C in glycosidic bonds (Espinosa-Andrews et al., 2010), the one at 1013 cm^{-1} attributed to C—O stretching of alcoholic groups in GA and CFR (Irfan et al., 2022), and the bands around 920 and 856 cm^{-1}, attributed to α-1,6-D-glycosidic bonds and CH2 deformation (Dai et al., 2019), respectively. The disappearance of these spectral bands can corroborate that the encapsulation process was effective, since the interactions between the components were effective and resulted in changes in the structure.

3.4. X-ray diffraction (XRD) measurements

XRD is widely used to analyze multicomponent samples and quantify the degree of crystallinity of materials (Arumugham et al., 2023). In microparticles, crystalline structures can confer greater stability and represent a key factor in modulating the release mechanisms of bioactive agents (Arumugham et al., 2023; Niyom et al., 2019). The Fig. 2**c** shows the XRD diffractograms of the different samples. SDT3/T4 presented similar profiles, with a semicrystalline-amorphous peak (2Θ of ~ 19.34°), a small protuberance around 2Θ of ~ 37.32° and a degree of crystallinity of 20.79 and 22.17, respectively, confirming its amorphous character. This occurs because GA, the main structural material,

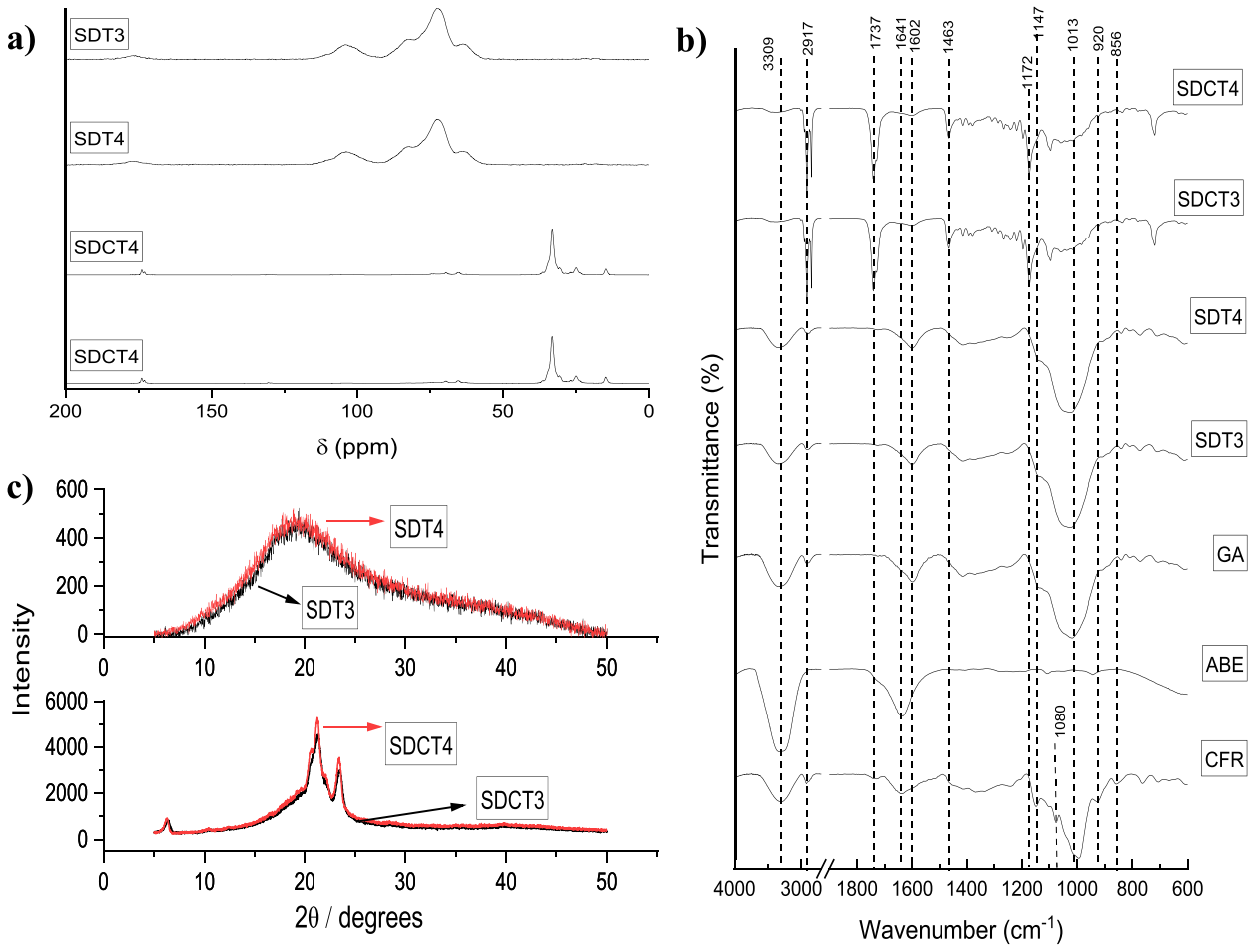

Fig. 2. a) ^{13}C CP/MAS NMR, b) Fourier transform infrared spectra (FT-IR), and c) X-ray diffractogram (XRD). SDT3 (CRF: 9.94g, ABE: 0.29g, AG: 39.25g), SDT4 (CRF: 9.94g, ABE: 0.44g, AG: 39.13g), and (SDCT3/T4), composed of a mixture of vegetable fat (FV), hydrogenated palm oil (HPO) and particles (SDT3 or SDT4), and 4.0 g o f polyglycerol polyricinoleate (PGPR), in a ratio of 1:2:2:0.2. ABE (*araçá-boi* extract), CRF (*cará-roxo* flour), and GA (gum arabic).

contains complex arabinogalactans that prevent the formation of ordered crystals. It is worth mentioning that amorphous samples are more hygroscopic, can become sticky or form agglomerates, which results in greater susceptibility to nutrient degradation, microstructure collapse and potential microbiological instability (Mahdi et al., 2020a). However, amorphous structures can improve the solubility, antioxidant activity and bioavailability of phenolics (Choi et al., 2022). In contrast, SDCT3/T4, obtained by combined encapsulation, presented similar profiles, with a degree of crystallinity of 29.36 and 28.81, respectively. Fig. 2**a** shows two more intense diffraction peaks (2Θ ~ 21.24; 23.44°), which highlights the predominance of β' triglyceride crystals (Fadini et al., 2021; Santos et al., 2023). Crystals with a β' structure are organized in an orthorhombic subcell, with interlayer spacing intermediate between the α and β forms (Fadini et al., 2021). This results in a more open and less dense structure, which increases compatibility with the bioactive compound carried, promotes gradual release, improves texture and palatability (Fadini et al., 2021). A third peak of lesser intensity at ~ 6.34° was detected in the SDCT3/T4 standards. This peak can be attributed to the presence of 1,2-dioleoyl-3-palmitoyl-*rac*-glycerol (OOP), a triacylglycerol that represents half of the molecular species of palm oil and has a crystalline structure in the α and β′ forms (Zhang et al., 2007). Based on the results, it was observed that the SDCT3/T4 samples exhibited superior crystallinity compared to the SDT3/T4 samples. This is in line with the findings by Santos et al. (2023), who also employed a combination of spray drying and spray chilling techniques to encapsulate β-carotene and obtained similar results.

3.5. Thermal analysis

DSC was used to characterize the thermodynamic properties of the microparticles (Fig. 3**a, b**). SDT3 showed an intense and thin exothermic peak at ~ 55 °C, suggesting sample rupture (Farshchi et al., 2019). As the temperature increased, internal pressurization caused expansion of the adsorbed free water, which resulted in the breakdown of the structure. Similar behavior has been observed in other microparticles by SD (Devi et al., 2023; Ugwu et al., 2022). SDT4 did not present any rupture in its structure, which can be attributed to the greater amount of ABE, which acted as a thermal reinforcement of the encapsulating structure, due to the formation of protein–polyphenol complexes (Pham et al., 2019). An endothermic event was observed around 47 °C, possibly related to T_g, indicating relaxation of the intermolecular hydrogen bonds of the SDT3/T4 chains. Between 80 and 120 °C, water evaporation from the material occurred, while at ~ 150 °C another glass transition was observed. These results indicated that SDT3/T4 can be stored at temperatures of up to 40 °C without compromising material properties, such as changes in structure or decreased stability. Similar stability temperatures were found in grape skin phenolic extract encapsulated with GA by spray drying (42 °C) and in *Eugenia stipitata* pulp encapsulated with maltodextrin by SD (42 °C) (Iturri et al., 2021; Kuck & Noreña, 2016). The SDCT3/T4 samples showed similar thermograms, with an intense endothermic event, starting at 35.04 °C and ending with a peak at 56.63 °C, which indicates the fusion of vegetable fat (VF) and hydrogenated palm oil (HPO), respectively. A similar result was observed in

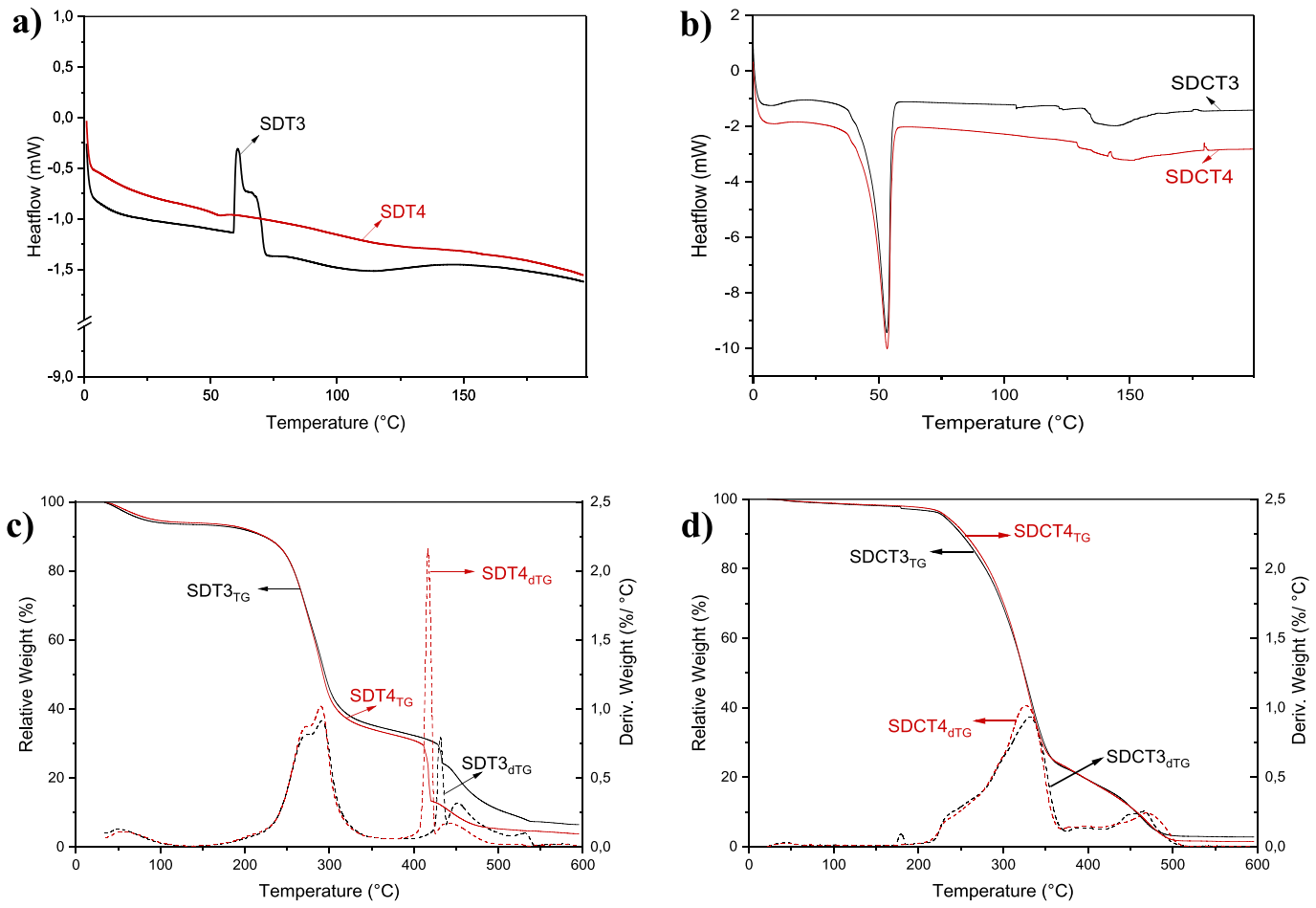

Fig. 3. Differential scanning calorimetry (DSC) of particles a) SDT3/T4, b) SDCT/T4 and thermogravimetric analysis (TGA) of particles c) SDT3/T4, d) SDCT/T4. Spray drying particles SDT3 (CRF: 9.94g, ABE: 0.29g, AG: 39.25g) and SDT4 (CRF: 9.94g, ABE: 0.44g, AG: 39.13g). Spray chilling multilayer particles (SDCT3/T4), being composed of a mixture of vegetable fat (FV), hydrogenated palm oil (HPO) and particles (SDT3 or SDT4), and 4.0 g of polyglycerol polyricinoleate (PGPR), in the proportion of 1:2:2:0.2. ABE (*araçá-boi* extract), CRF (*cará-roxo* flour) and GA (gum arabic).

microparticles loaded with fish oil, also using the combination of FV and HPO (Fadini et al., 2021). Mixing lipids to the particle wall by SDC resulted in a point that lies between the fusion of FV and HPO. This was achieved due to the heterogeneous distribution of different types of triacylglycerols (TAGs), which favored the formation of β' crystals, responsible for the intermediate melting point (Fadini et al., 2021; Santos et al., 2023). SDCT3 and SDCT4 showed water evaporation at around 130 °C, which may be due to SD microparticles, after the fusion of the lipid wall (Ferreira Nogueira et al., 2018). Subsequently, a T_g ~ 150 °C was observed, more pronounced in SDCT4, like the single-walled samples (SDT3/T4). A similar T_g condition has been reported (Ferreira Nogueira et al., 2018). Two low-intensity exothermic peaks (142.64–179.71 °C) were observed in SDCT4, which may have been caused by the degradation of hydrogen bonds between FV unsaturated fatty acid molecules. The comparison of encapsulation by SD and SDC showed significant differences in thermodynamic properties, with emphasis on double-layer microparticles, which prevented structure rupture, resulting in greater thermal stability of the samples.

The thermal stability of microparticles for programmed sequential release of phenolics was tested using TGA, as illustrated in (Fig. 3**c, d**). According to the thermographs obtained, SDT3/T4 presented five and four mass loss events, respectively, and a similar thermal behavior, recorded in the temperature range from 0 to 600 °C. Both SD microparticles showed an initial peak around 51.91 °C, ending at 150 °C, with a mass loss of approximately 5%, which was attributed to moisture removal (Hellebois et al., 2023). In the temperature range of 204.31–351.3 °C, the mass loss was mainly associated with the cleavage of saccharide rings, the disintegration of macromolecular chains and the volatilization of partial compounds of the CRF-GA structure (Wang et al., 2023). Two intense and thin peaks around 432.19 °C (SDT3) and 417.28 °C (SDT4) may be related to the pyrolysis and volatilization of phenolic compounds (PC) (Chen et al., 2023), with more pronounced mass loss in SDT4 (87.53%) than in SDT3 (32.10%), which can be explained by the lower amount of PC in SDT3, since the amount of ABE was reduced by 0.44 g (SDT4) to 0.29 g. Final stage carbonization occurred between 450 and 550 °C, similar to the results of Wang et al. (2023), when they encapsulated curcumin using gliadin and chitosan hydrochloride. SDCT3/T4 showed degradation distributed in two main stages. The peaks were similar, except at 179.38 °C, which showed an exclusive peak for SDCT3, related to a small loss of adsorbed water (2.8%). After this, a broad peak between 200 and 400 °C can be attributed to the decomposition of triglycerides, the main components of FV and HPO, followed by another peak related to the decomposition of free fatty acids (450–500 °C) (Flávia Justino Uchoa et al., 2021).

Combining the results from DSC, TGA and FTIR, the strong interaction between CRF-GA and FV-HPO generated a thick and dense interfacial layer structure, indicating that SD or SDC samples are thermally stable up to temperatures of ~ 47 °C. However, SDCT3/T4 are more thermally stable than SDT3/T4 samples, as the lipids in SDCT3/T4 samples do not easily induce the thermal degradation of other sample components, including PC.

3.6. In vitro digestion and antioxidant capacity

Fig. 4 shows the concentration of phenolic compounds (PC) found by UPLC-ESI-QTOF-MS analysis in the different phases of *in vitro* digestion. PC come directly from CRF and/or ABE, being classified into three subclasses: flavonol (quercetin, rutin, myricetin and kaempferol) and hydroxycinnamic acid (chlorogenic and protocatechuic acid) and cinnamic acid (ferrulic, *p*-coumaric and *trans*-cinnamic) (**Material Supplementary 3**) (Adomėnienė & Venskutonis, 2022). In pre-digestion, PC release was limited by solubility in aqueous media, being relatively low ($\leq$0.02 mg g^{-1}) and less pronounced in SDCT3/T4, except for *trans*-cinnamic acids (0.42 mg g^{-1}) and protocatechuic (0.07 mg g^{-1}) in the SD samples (SDT3/T4), in addition to rutin (0.08 mg g^{-1}) in SDT4. Especially, *trans*-cinnamic acid had immediate release in hydro-interaction (SDT3/T4), not being found in later phases. In gastric phase, SD released more PC than in the intestinal phase, being higher than in SDCT3/T4, due to the hydrolysis of the glycosidic bonds in the CRF-GA wall in an acidic environment, which suggests good protection of the double layer (SDC) (Shrotri et al., 2017). Chlorogenic acid (SDT3: 0.03 mg g^{-1}; SDT4: 0.09 mg g^{-1}) and rutin (SDT3: 0.04 mg g^{-1}; SDT4: 0.04 mg g^{-1}) had higher release in the gastric phase, which may be related to the greater protonation capacity and solubility of these compounds (Asadi et al., 2019). SDT3-gastric showed a significant release of gallic acid (0.03 mg g^{-1}), demonstrating that a smaller amount of ABE does not induce the formation of protein–polyphenol complexes, resulting in lower stability (Pham et al., 2019). During the intestinal phase SDC microparticles showed better performance compared to previous phases, and, for some phenolics, the release was greater than in SD microparticles, with emphasis on chlorogenic acid, which showed intestinal release (SDCT3/T4, ~0.02 mg g-1), with a significant difference ($p < 0.05$) in SDT3/T4. However, SD microparticles also show good intestinal release, *e.g.*, rutin (0.03 mg g-1) in SDT4, showing that the structure designed with CRF-GA conferred good bioaccessibility of PCs (Santos et al., 2023) when encapsulating β-carotene via SDC, and reported that the presence of lipids combined with GA may hinder the bioaccessibility of double-layer microparticles. In addition, the fatty acid composition of the lipid carrier can affect bioaccessibility, indicating that higher levels of monounsaturated fatty acids (*e.g.*, oleic acid) are more efficient in forming double-layer walls than saturated long-chain fatty acids, such as palmitic acid present in HPO (Santos et al., 2023).

The antioxidant capacity (AC) of the *in vitro* digestion phases was determined by ORAC and ABTS (Fig. 5). Initially, there was a difference in AC values by ABTS and ORAC, which can be explained by the selectivity of the ABTS radical for PC, unlike ORAC, which is a method that covers other types of antioxidant compounds (Munteanu & Apetrei, 2021). In the pre-digestion phase the samples showed lower CA with emphasis on SDCT3/T4, which ranged from 0.46 to 3.37 μmol TE g^{-1}, indicating good incorporation of PCs in the multilayer co-delivery

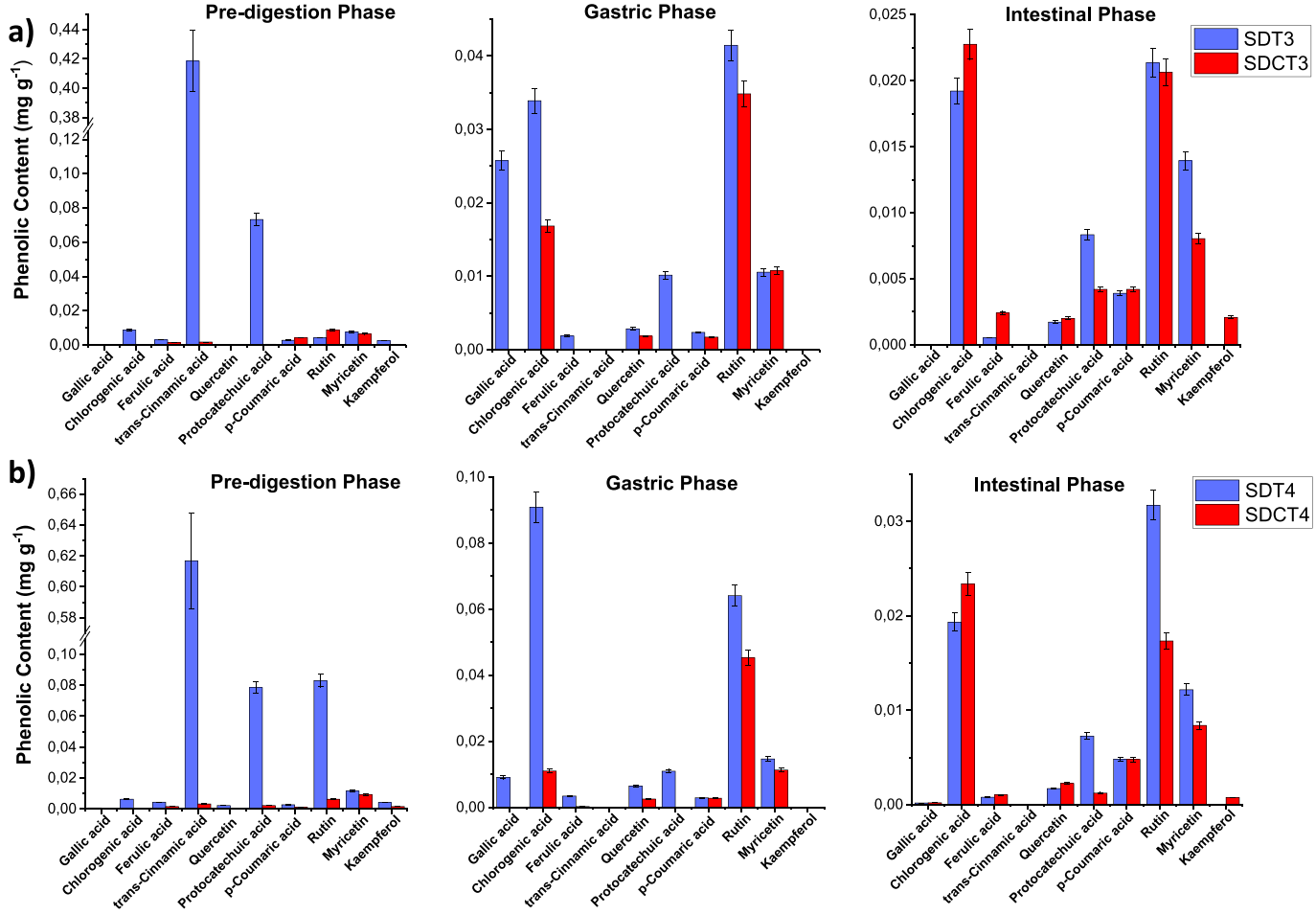

Fig. 4. Concentration of phenolic compounds (mg g^{-1}) in *in vitro* static digestion. Lowercase letters indicate that the means are significantly ($p < 0.05$) different by Tukey, when comparing different processes: a) SDT3-SDCT3 and b) SDT4-SDCT4. Different uppercase letters indicate that the means are significantly different ($p < 0$, 05) between particles (SDT3, SDT4, SDSCT3, SDSCT4) in each digestion phase (pre-digestion, gastric and intestinal). SDT3 (CRF: 9.94g, ABE: 0.29g, AG: 39.25g) and SDT4 (CRF: 9.94g, ABE: 0.44g, AG: 39.13g). Spray chilling multilayer particles (SDCT3/T4), being composed of a mixture of vegetable fat (FV), hydrogenated palm oil (HPO) and particles (SDT3 or SDT4), and 4.0 g of polyglycerol polyricinoleate (PGPR), in the proportion of 1:2:2:0.2. ABE (*araçá-boi* extract), CRF (*cará-roxo* flour) and GA (gum arabic).

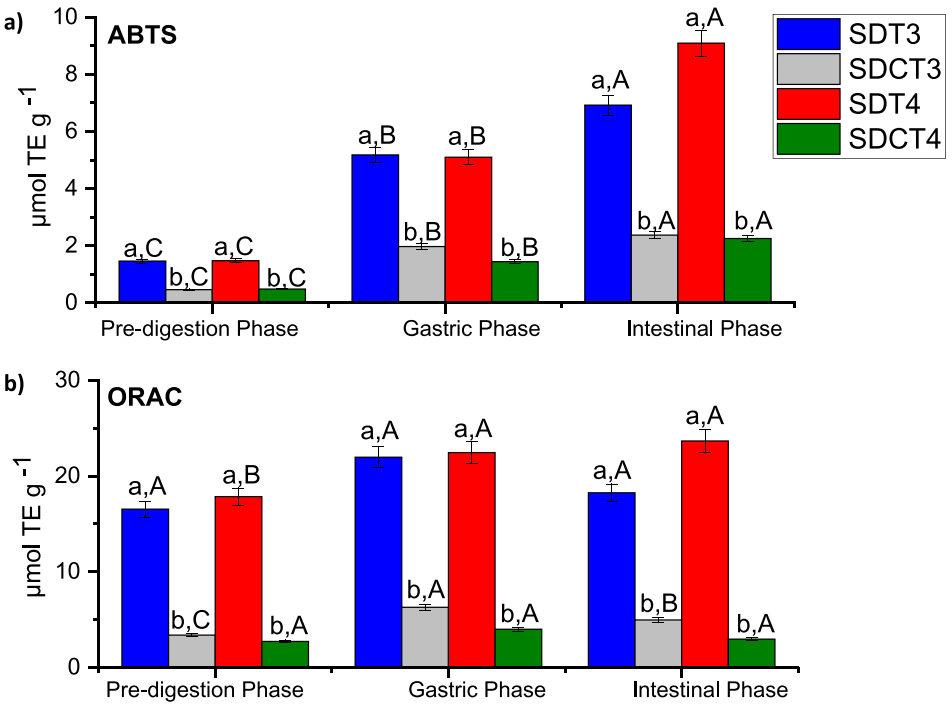

Fig. 5. Concentration of phenolic compounds (mg g^{-1}) in in vitro static digestion. Lowercase letters indicate that the means are significantly ($p < 0.05$) different by Tukey, when comparing different processes: a) SDT3-SDCT3 and b) SDT4-SDCT4. Different uppercase letters indicate that the means are significantly different ($p < 0.05$) between particles (SDT3, SDT4, SDSCT3, SDSCT4) in each digestion phase (pre-digestion, gastric and intestinal). SDT3 (CRF: 9.94g, ABE: 0.29g, AG: 39.25g) and SDT4 (CRF: 9.94g, ABE: 0.44g, AG: 39.13g). Spray chilling multilayer particles (SDCT3/T4), being composed of a mixture of vegetable fat (FV), hydrogenated palm oil (HPO) and particles (SDT3 or SDT4), and 4.0 g of polyglycerol polyricinoleate (PGPR), in the proportion of 1:2:2:0.2. ABE (*araçá-boi* extract), CRF (*cará-roxo* flour) and GA (gum arabic).

system. In the gastric phase there was an increase in AC for all samples, reaching a maximum of 22.46 μmol TE g^{-1} (ORAC) in SDT4, opposite to its analogue (SDCT4), which presented a lower AC (3.99 μmol TE g^{-1}, ORAC). This may indicate greater protection of antioxidants against the action of simulated gastric juice in SDC (Fadini et al., 2019). In the intestinal phase, SD microparticles showed higher AC, reaching the maximum value in SDT4 (23.66 μmol TE g^{-1}, ORAC), in agreement with the UPLC-ESI-QTOF-MS analysis, which detected for this same sample, the highest phenolic concentration (0.03 mg g^{-1}) related to rutin. Furthermore, the results showed lower SDCT3/T4 antioxidant capacity, although there was an increase in CA in the intestinal phase, which may suggest that the stable structure of SDC releases antioxidants in a sustained manner, as reported by Figueiredo et al. (2022). The controlled release of antioxidant compounds can be beneficial to optimize absorption and prolong their effects in the human body (Figueiredo et al., 2022).

4. Conclusions

PCs were successfully microencapsulated by SD and SDC in a pioneering way, demonstrating high retention of phenolics, especially for protocatechuic, *trans*-cinnamic and ferulic acids. The materials obtained presented desirable characteristics of microstructure, size distribution and crystallinity that can facilitate manipulation, incorporation, and stability in foods. NMR and FTIR confirmed the presence of key-components and interactions within the microparticles. XRD analysis showed greater stability in SDCT3/T4, evidenced by crystalline structures, and thermal analyzes indicated that SD or SDC were stable at temperatures up to ~ 47 °C. *In vitro* digestion revealed differences in PC release. SDC microparticles showed better protection of phenolic compounds during the gastric phase and had their best performance in the intestinal phase. However, SD particles also showed excellent intestinal release and greater antioxidant capacity than SDC, suggesting that more studies are needed to better understand the influence of the composition of wall materials and the controlled release kinetics of PC in SDC during simulated digestion.

Ethical approval

This article does not contain any studies with human participants or animals performed by any of the authors.

CRediT authorship contribution statement

Williara Queiroz de Oliveira: Writing – review & editing, Writing – original draft, Visualization, Validation, Supervision, Software, Project administration, Methodology, Investigation, Formal analysis, Data curation, Conceptualization. **Iramaia Angélica Neri Numa:** Methodology, Conceptualization, Supervision, Writing – review & editing. **Izabela D. Alvim:** Writing – review & editing, Visualization, Investigation, Conceptualization. **Henriette M.C. Azeredo:** Writing – review & editing, Writing – original draft, Visualization, Methodology, Conceptualization. **Leticia B. Santos:** Software, Methodology, Investigation. **Felipe T. Borsoi:** Software, Methodology, Investigation. **Fábio F. de Araújo:** Software, Methodology. **Alexandra C.H.F. Sawaya:** Methodology, Data curation. **Gustavo C. do Nascimento:** Methodology. **Maria Teresa P.S. Clerici:** Methodology. **Célio K. do Sacramento:** Visualization. **Glaucia Maria Pastore:** Project administration, Resources, Supervision.

Declaration of Competing Interest

The authors declare that they have no known competing financial interests or personal relationships that could have appeared to influence the work reported in this paper.

Data availability

No data was used for the research described in the article.

Acknowledgments

The authors would like to thank the National Council for Scientific and Technological Development (CNPq, grant numbers 406820/2018-0; 159123/2019-4), São Paulo Research Foundation (FAPESP, grant numbers 2020/08761-4) and Coordination for the Improvement of Higher Education Personnel (CAPES) – Finance Code 001 for their financial support. The authors also would like to thank B. L. Tagliapietra, P. H. Campelo, G. C. Nascimento and M. T. P. Clerici for donating the cará-roxo flour, and to ITAL for donating the arabic gum. The authors would also thank Camila D. Gonçalves and Maria Júlia D.P. Santos for extracting the ABE. W.Q. de Oliveira would like to thank National Council for Scientific and Technological Development (CNPq, grant number 142316/2019-9) and the Unicamp Development Foundation, through *Auxílio Ponte* (through agreement n° 519,292, Item: 1001, Faepex Scholarship). H.M.C. Azeredo would like to thank the National Council for Scientific and Technological Development (CNPq) for her Research Productivity Fellowship (308777/2021-2). A.C.H.F. Sawaya and L.B. Santos would like to thank CNPq grant n° 306100/2021-5 and 130182/2020-6, respectively. F. F. de Araújo (grant# 2020/15163-6 and 2022/04530-3) would like to thank FAPESP. M. T. P. Clerici would like to thank CAPES - Coordination for the Improvement of Higher Education Personnel (n° 312786/2020-4), and the Cargill Foundation (process 5610 - Tubers), as well as the City Administration of Caapiranga (AM, Brazil). G. C. Nascimento (Process no. 88887.605707/2021-00), would like to thank the Fund to Support Teaching, Research, and Extension - Faepex (2679/21), the Cargill Foundation (process 5610 – Tubérculos), as well as the City Administration of Caapiranga (AM, Brazil).

Declaration of generative AI in scientific writing

The authors did not use generative artificial intelligence (AI) or AI-assisted technologies in the writing process.

Appendix A. Supplementary data

Supplementary data to this article can be found online at https://doi.org/10.1016/j.foodchem.2024.138579.

References

Adomėnienė, A., & Venskutonis, P. R. (2022). Dioscorea spp.: Comprehensive Review of Antioxidant Properties and Their Relation to Phytochemicals and Health Benefits. In *Molecules*. https://doi.org/10.3390/molecules27082530.

Aguiar, E. V., Santos, F. G., Krupa-Kozak, U., & Capriles, V. D. (2023). Nutritional facts regarding commercially available gluten-free bread worldwide: Recent advances and future challenges. *Critical Reviews in Food Science and Nutrition, 63*(5), 693–705. https://doi.org/10.1080/10408398.2021.1952403

Alvim, I. D., Stein, M. A., Koury, I. P., Dantas, F. B. H., & Cruz, C. L. de C. V. (2016). Comparison between the spray drying and spray chilling microparticles contain ascorbic acid in a baked product application. *LWT - Food Science and Technology*. https://doi.org/10.1016/j.lwt.2015.08.049.

Amirabadi, S., Milani, J. M., & Sohbatzadeh, F. (2020). Application of dielectric barrier discharge plasma to hydrophobically modification of gum arabic with enhanced surface properties. *Food Hydrocolloids, 104*, Article 105724. https://doi.org/10.1016/j.foodhyd.2020.105724

Andrew, J., Masetlwa, J., Tesfaye, T., & Sithole, B. (2020). Beneficiation of eucalyptus tree barks in the context of an integrated biorefinery – Optimisation of accelerated solvent extraction (ASE) of polyphenolic compounds using response surface methodology. *Sustainable Chemistry and Pharmacy*. https://doi.org/10.1016/j.scp.2020.100327

Angelo, P. M., & Jorge, N. (2007). *Phenolic compounds in foods – A brief review*. Revista Do Instituto Adolfo Lutz.

Antony, A., & Farid, M. (2022). Effect of Temperatures on Polyphenols during Extraction. *Applied Sciences, 12*(4), 2107. https://doi.org/10.3390/app12042107

Arumugham, T., Krishnamoorthy, R., AlYammahi, J., Hasan, S. W., & Banat, F. (2023). Spray dried date fruit extract with a maltodextrin/gum arabic binary blend carrier agent system: Process optimization and product quality. *International Journal of Biological Macromolecules, 238*, Article 124340. https://doi.org/10.1016/j.ijbiomac.2023.124340

Asadi, N., Ramezanzadeh, M., Bahlakeh, G., & Ramezanzadeh, B. (2019). Utilizing Lemon Balm extract as an effective green corrosion inhibitor for mild steel in 1M HCl solution: A detailed experimental, molecular dynamics, Monte Carlo and quantum mechanics study. *Journal of the Taiwan Institute of Chemical Engineers, 95*, 252–272. https://doi.org/10.1016/j.jtice.2018.07.011

Asranudin, Holilah, Syarifin, A. N. K., Purnomo, A. S., Ansharullah, & Fudholi, A. (2021). The effect of heat moisture treatment on crystallinity and physicochemical-digestibility properties of purple yam flour. *Food Hydrocolloids*, *120*, 106889. https://doi.org/10.1016/j.foodhyd.2021.106889.

Badawi, N. M., Attia, Y. M., El-Kersh, D. M., Hammam, O. A., & Khalifa, M. K. A. (2022). Investigating the Impact of Optimized Trans-Cinnamic Acid-Loaded PLGA Nanoparticles on Epithelial to Mesenchymal Transition in Breast Cancer. *International Journal of Nanomedicine*. https://doi.org/10.2147/IJN.S345870

Bajac, J., Nikolovski, B., Lončarević, I., Petrović, J., Bajac, B., Đurović, S., & Petrović, L. (2022). Microencapsulation of juniper berry essential oil (Juniperus communis L.) by spray drying: Microcapsule characterization and release kinetics of the oil. *Food Hydrocolloids.*. https://doi.org/10.1016/j.foodhyd.2021.107430

Banožić, M., Čolnik, M., Škerget, M., Cikoš, A.-M., Aladić, K., & Jokić, S. (2022). Formation and Characterization of Fucus virsoides J. Agardh Pigment-Polyethylene Glycol Microparticles Produced Using PGSS Process. *Applied Sciences, 12*(22), 11496. https://doi.org/10.3390/app122211496

Bera, H., Hossain, C. M., & Saha, S. (2021). Biopolymer-Based Nanomaterials in Drug Delivery and Biomedical Applications. *In Biopolymer-Based Nanomaterials in Drug Delivery and Biomedical Applications*. https://doi.org/10.1016/C2019-0-02043-2

Chen, N., Gao, H. X., He, Q., & Zeng, W. C. (2023). Potential application of phenolic compounds with different structural complexity in maize starch-based film. *Food Structure*. https://doi.org/10.1016/j.foostr.2023.100318

Choi, I., Li, N., & Zhong, Q. (2022). Co-loading curcumin and quercetin in freeze-dried mushroom microparticles to inhibit lipid oxidation in beef patties. *Food Chemistry*. https://doi.org/10.1016/j.foodchem.2021.131625

Comunian, T. A., Boillon, M. R. G., Thomazini, M., Nogueira, M. S., de Castro, I. A., & Favaro-Trindade, C. S. (2016). Protection of echium oil by microencapsulation with phenolic compounds. *Food Research International*. https://doi.org/10.1016/j.foodres.2016.03.008

Cutrim, C. S., Alvim, I. D., & Cortez, M. A. S. (2019). Microencapsulation of green tea polyphenols by ionic gelation and spray chilling methods. *In Journal of Food Science and Technology*. https://doi.org/10.1007/s13197-019-03908-1

Dai, L., Zhang, J., & Cheng, F. (2019). Effects of starches from different botanical sources and modification methods on physicochemical properties of starch-based edible films. *International Journal of Biological Macromolecules, 132*, 897–905. https://doi.org/10.1016/j.ijbiomac.2019.03.197

de Araújo, F. F., de Paulo Farias, D., Neri-Numa, I. A., Dias-Audibert, F. L., Delafiori, J., de Souza, F. G., et al. (2021a). Chemical characterization of Eugenia stipitata: A native fruit from the Amazon rich in nutrients and source of bioactive compounds. *Food Research International*. https://doi.org/10.1016/j.foodres.2020.109904

de Araújo, F. F., de Paulo Farias, D., Neri-Numa, I. A., Dias-Audibert, F. L., Delafiori, J., de Souza, F. G., et al. (2021b). Gastrointestinal bioaccessibility and bioactivity of phenolic compounds from araçá-boi fruit. *LWT*. https://doi.org/10.1016/j.lwt.2020.110230

de Araújo, F. F., Neri-Numa, I. A., de Paulo Farias, D., da Cunha, G. R. M. C., & Pastore, G. M. (2019). Wild Brazilian species of Eugenia genera (Myrtaceae) as an innovation hotspot for food and pharmacological purposes. *In Food Research International*. https://doi.org/10.1016/j.foodres.2019.03.018

Devi, L. M., Das, A. B., & Badwaik, L. S. (2023). Effect of gelatin and acacia gum on anthocyanin coacervated microcapsules using double emulsion and its characterization. *International Journal of Biological Macromolecules*. https://doi.org/10.1016/j.ijbiomac.2023.123896

Di Pietro, M. E., Mannu, A., & Mele, A. (2020). NMR determination of free fatty acids in vegetable oils. *In Processes*. https://doi.org/10.3390/PR8040410

Dong, L., Sun, X., Chao, Z., Zhang, S., Zheng, J., Gurung, R., Du, J., Shi, J., Xu, Y., Zhang, Y., & Wu, J. (2014). Evaluation of FTIR spectroscopy as diagnostic tool for colorectal cancer using spectral analysis. *Spectrochimica Acta Part A: Molecular and Biomolecular Spectroscopy, 122*, 288–294. https://doi.org/10.1016/j.saa.2013.11.031

Espinosa-Andrews, H., Sandoval-Castilla, O., Vázquez-Torres, H., Vernon-Carter, E. J., & Lobato-Calleros, C. (2010). Determination of the gum Arabic–chitosan interactions by Fourier Transform Infrared Spectroscopy and characterization of the microstructure and rheological features of their coacervates. *Carbohydrate Polymers, 79*(3), 541–546. https://doi.org/10.1016/j.carbpol.2009.08.040

Fadini, A. L., Alvim, I. D., Carazzato, C. A., Paganotti, K. B. de F., Miguel, A. M. R. de O., & Rodrigues, R. A. F. (2021). Microparticles loaded with fish oil: stability studies, food application and sensory evaluation. *Journal of Microencapsulation*. https://doi.org/10.1080/02652048.2021.1948622.

Fadini, A. L., Alvim, I. D., Ribeiro, I. P., Ruzene, L. G., da Silva, L. B., Queiroz, M. B., et al. (2018). Innovative strategy based on combined microencapsulation technologies for food application and the influence of wall material composition. *LWT*. https://doi.org/10.1016/j.lwt.2018.01.071

Fadini, A. L., Dutra Alvim, I., Paganotti, K. B. de F., Bataglia da Silva, L., Bonifácio Queiroz, M., Miguel, A. M. R. de O., & Rodrigues, R. A. F. (2019). Optimization of the production of double-shell microparticles containing fish oil. *Food Science and Technology International*, *25*(5), 359–369. https://doi.org/10.1177/1082013219825890.

Farshchi, A., Hassanpour, A., & Bayly, A. E. (2019). The structure of spray-dried detergent powders. *Powder Technology*. https://doi.org/10.1016/j.powtec.2019.06.049

Favaro-Trindade, C. S., de Matos Junior, F. E., Okuro, P. K., Dias-Ferreira, J., Cano, A., Severino, P., Zielińska, A., & Souto, E. B. (2021). Encapsulation of active pharmaceutical ingredients in lipid micro/nanoparticles for oral administration by spray-cooling. *In Pharmaceutics*. https://doi.org/10.3390/pharmaceutics13081186

Fernandes de Araújo, F., de Paulo Farias, D., Neri-Numa, I. A., Dias-Audibert, F. L., Delafiori, J., Gama de Souza, F., et al. (2020). Gastrointestinal bioaccessibility and bioactivity of phenolic compounds from araçá-boi fruit. *LWT, 110230*. https://doi.org/10.1016/j.lwt.2020.110230.

Ferreira Nogueira, G., Pereira Martin, L. G., Matta Fakhouri, F., & Augustus de Oliveira, R. (2018). Microencapsulation of blackberry pulp with arrowroot starch and gum arabic mixture by spray drying. *Journal of Microencapsulation*. https://doi.org/10.1080/02652048.2018.1538264

Figueiredo, J. de A., Silva, C. R. de P., Souza Oliveira, M. F., Norcino, L. B., Campelo, P. H., Botrel, D. A., & Borges, S. V. (2022). Microencapsulation by spray chilling in the food industry: Opportunities, challenges, and innovations. In *Trends in Food Science and Technology*. https://doi.org/10.1016/j.tifs.2021.12.026.

Flávia Justino Uchoa, A., da Silva Rocha, W., Peter Macedo Feitosa, J., Lopes Nogueira, R., Hellen Almeida de Brito, D., Barbosa Soares, J., & de Aguiar Soares, S. (2021). Bio-based palm oil as an additive for asphalt binder: Chemical characterization and rheological properties. *Construction and Building Materials*, *285*, 122883. https://doi.org/10.1016/j.conbuildmat.2021.122883.

Funami, T., Nakauma, M., Ishihara, S., Tanaka, R., Inoue, T., & Phillips, G. O. (2011). Structural modifications of sugar beet pectin and the relationship of structure to functionality. *Food Hydrocolloids*. https://doi.org/10.1016/j.foodhyd.2009.11.017

Goksen, G., Demir, D., Dhama, K., Kumar, M., Shao, P., Xie, F., Echegaray, N., & Lorenzo, J. M. (2023). Mucilage polysaccharide as a plant secretion: Potential trends in food and biomedical applications. *International Journal of Biological Macromolecules, 230*, Article 123146. https://doi.org/10.1016/j.ijbiomac.2023.123146

Hatefi, L., & Farhadian, N. (2020). A safe and efficient method for encapsulation of ferrous sulfate in solid lipid nanoparticle for non-oxidation and sustained iron delivery. *Colloids and Interface Science Communications*. https://doi.org/10.1016/j.colcom.2019.100227

Hellebois, T., Addiego, F., Gaiani, C., Shaplov, A. S., & Soukoulis, C. (2023). Unravelling the functionality of anionic and non-ionic plant seed gums on milk protein cryogels conveying Lacticaseibacillus rhamnosus GG. *Carbohydrate Polymers, 121376*. https://doi.org/10.1016/j.carbpol.2023.121376

Hernández-Barrueta, T., Martínez-Bustos, F., Castaño-Tostado, E., Lee, Y., Miller, M. J., & Amaya-Llano, S. L. (2020). Encapsulation of probiotics in whey protein isolate and modified huauzontle's starch: An approach to avoid fermentation and stabilize polyphenol compounds in a ready-to-drink probiotic green tea. *LWT*. https://doi.org/10.1016/j.lwt.2020.109131

Human, C., De Beer, D., Van Der Rijst, M., Aucamp, M., & Joubert, E. (2019). Electrospraying as a suitable method for nanoencapsulation of the hydrophilic bioactive dihydrochalcone, aspalathin. *Food Chemistry*. https://doi.org/10.1016/j.foodchem.2018.10.016

Irfan, M., Munir, H., & Ismail, H. (2022). Characterization and fabrication of zinc oxide nanoparticles by gum Acacia modesta through green chemistry and impregnation on surgical sutures to boost up the wound healing process. *International Journal of Biological Macromolecules, 204*, 466–475. https://doi.org/10.1016/j.ijbiomac.2022.02.043

Isobe, N., Sagawa, N., Ono, Y., Fujisawa, S., Kimura, S., Kinoshita, K., Miuchi, T., Iwata, T., Isogai, A., Nishino, M., & Deguchi, S. (2020). Primary structure of gum arabic and its dynamics at oil/water interface. *Carbohydrate Polymers, 249*, Article 116843. https://doi.org/10.1016/j.carbpol.2020.116843

Iturri, M. S., Calado, C. M. B., & Prentice, C. (2021). Microparticles of Eugenia stipitata pulp obtained by spray-drying guided by DSC: An analysis of bioactivity and in vitro gastrointestinal digestion. *Food Chemistry*, *334*(February 2020), 127557. https://doi.org/10.1016/j.foodchem.2020.127557.

Karaaslan, M., Şengün, F., Cansu, Ü., Başyiğit, B., Sağlam, H., & Karaaslan, A. (2021). Gum arabic/maltodextrin microencapsulation confers peroxidation stability and antimicrobial ability to pepper seed oil. *Food Chemistry*. https://doi.org/10.1016/j.foodchem.2020.127748

Kuck, L. S., & Noreña, C. P. Z. (2016). Microencapsulation of grape (Vitis labrusca var. Bordo) skin phenolic extract using gum Arabic, polydextrose, and partially hydrolyzed guar gum as encapsulating agents. *Food Chemistry, 194*, 569–576. https://doi.org/10.1016/j.foodchem.2015.08.066

Li, T., Wan, B., Jog, R., Costa, A., & Burgess, D. J. (2022). Pectin microparticles for peptide delivery: Optimization of spray drying processing. *International Journal of Pharmaceutics, 613*, Article 121384. https://doi.org/10.1016/j.ijpharm.2021.121384

Lopez-Polo, J., Silva-Weiss, A., Giménez, B., Cantero-López, P., Vega, R., & Osorio, F. A. (2020). Effect of lyophilization on the physicochemical and rheological properties of food grade liposomes that encapsulate rutin. *Food Research International*. https://doi.org/10.1016/j.foodres.2019.108967

Machado, M. H., Almeida, A. da R., Maciel, M. V. de O. B., Vitorino, V. B., Bazzo, G. C., da Rosa, C. G., et al. (2022). Microencapsulation by spray drying of red cabbage anthocyanin-rich extract for the production of a natural food colorant. *Biocatalysis and Agricultural Biotechnology*. https://doi.org/10.1016/j.bcab.2022.102287.

Mahdi, A. A., Mohammed, J. K., Al-Ansi, W., Ghaleb, A. D. S., Al-Maqtari, Q. A., Ma, M., Ahmed, M. I., & Wang, H. (2020a). Microencapsulation of fingered citron extract with gum arabic, modified starch, whey protein, and maltodextrin using spray drying. *International Journal of Biological Macromolecules*. https://doi.org/10.1016/j.ijbiomac.2019.10.201

Mahdi, A. A., Mohammed, J. K., Al-Ansi, W., Ghaleb, A. D. S., Al-Maqtari, Q. A., Ma, M., Ahmed, M. I., & Wang, H. (2020b). Microencapsulation of fingered citron extract with gum arabic, modified starch, whey protein, and maltodextrin using spray drying. *International Journal of Biological Macromolecules, 152*, 1125–1134. https://doi.org/10.1016/j.ijbiomac.2019.10.201

Martínez, A., Mijangos, G. E., Romero-Ibarra, I. C., Hernández-Altamirano, R., Mena-Cervantes, V. Y., & Gutiérrez, S. (2018). A novel green one-pot synthesis of biodiesel from Ricinus communis seeds by basic heterogeneous catalysis. *Journal of Cleaner Production, 196*, 340–349. https://doi.org/10.1016/j.jclepro.2018.05.241

Mehran, M., Masoum, S., & Memarzadeh, M. (2020). Improvement of thermal stability and antioxidant activity of anthocyanins of Echium amoenum petal using maltodextrin/modified starch combination as wall material. *International Journal of Biological Macromolecules*. https://doi.org/10.1016/j.ijbiomac.2020.01.197

Mollica, J. Q., Cara, D. C., D'Auriol, M., Oliveira, V. B., Cesar, I. C., & Brandão, M. G. L. (2013). Anti-inflammatory activity of American yam Dioscorea trifida L.f. in food allergy induced by ovalbumin in mice. *Journal of Functional Foods.*. https://doi.org/10.1016/j.jff.2013.09.020

Munteanu, I. G., & Apetrei, C. (2021). Analytical Methods Used in Determining Antioxidant Activity: A Review. *International Journal of Molecular Sciences, 22*(7), 3380. https://doi.org/10.3390/ijms22073380

Ndiwe, B., Pizzi, A., Tibi, B., Danwe, R., Konai, N., & Amirou, S. (2019). African tree bark exudate extracts as biohardeners of fully biosourced thermoset tannin adhesives for wood panels. *Industrial Crops and Products*. https://doi.org/10.1016/j.indcrop.2019.02.023

Neri-Numa, I. A., Pessôa, M. G., Arruda, H. S., Pereira, G. A., Paulino, B. N., Angolini, C. F. F., Ruiz, A. L. T. G., & Pastore, G. M. (2020). Genipap (Genipa americana L.) fruit extract as a source of antioxidant and antiproliferative iridoids. *Food Research International, 134*, Article 109252. https://doi.org/10.1016/j.foodres.2020.109252

Neuenfeldt, N. H., de Moraes, D. P., de Deus, C., Barcia, M. T., & de Menezes, C. R. (2022). Blueberry Phenolic Composition and Improved Stability by Microencapsulation. *In Food and Bioprocess Technology*. https://doi.org/10.1007/s11947-021-02749-1

Niyom, Y., Phakkeeree, T., Flood, A., & Crespy, D. (2019). Synergy between polymer crystallinity and nanoparticles size for payloads release. *Journal of Colloid and Interface Science*. https://doi.org/10.1016/j.jcis.2019.04.085

de Oliveira, W. Q., Neri-Numa, I. A., Arruda, H. S., McClements, D. J., & Pastore, G. M. (2022). Encapsulation of flavonoids in foods for diabetics: The emerging paradigm for an effective therapy. *Trends in Food Science & Technology, 127*, 198–206. https://doi.org/10.1016/j.tifs.2022.06.004

Oliveira, W. Q. de, Wurlitzer, N. J., Araújo, A. W. de O., Comunian, T. A., Bastos, M. do S. R., Oliveira, A. L. de, et al. (2020). Complex coacervates of cashew gum and gelatin as carriers of green coffee oil: The effect of microcapsule application on the rheological and sensorial quality of a fruit juice. *Food Research International*, *131*, 109047. https://doi.org/10.1016/j.foodres.2020.109047.

Paulo, B. B., Ramos, F. de M., Feliciano, M. D., Prado, D. P., Silveira, M. P., Alvim, I. D., & Prata, A. S. (2022). Spherification of Hydrocolloids by Jet Cutter. *Journal of Culinary Science & Technology*, 1–14. https://doi.org/10.1080/15428052.2022.2077877.

Pereira de Oliveira, J., Almeida, O. P., Campelo, P. H., Carneiro, G., de Oliveira Ferreira Rocha, L., Santos, J. H. P. M., & Gomes da Costa, J. M. (2022). Tailoring the physicochemical properties of freeze-dried buriti oil microparticles by combining inulin and gum Arabic as encapsulation agents. *Lwt*, *161*(March). https://doi.org/10.1016/j.lwt.2022.113372.

Pham, L. B., Wang, B., Zisu, B., & Adhikari, B. (2019). Complexation between flaxseed protein isolate and phenolic compounds: Effects on interfacial, emulsifying and antioxidant properties of emulsions. *Food Hydrocolloids*. https://doi.org/10.1016/j.foodhyd.2019.03.007

Pinho, L. S., de Lima, P. M., de Sá, S. H. G., Chen, D., Campanella, O. H., da Costa Rodrigues, C. E., & Favaro-Trindade, C. S. (2022). Encapsulation of Rich-Carotenoids Extract from Guaraná (Paullinia cupana) Byproduct by a Combination of Spray Drying and Spray Chilling. *Foods, 11*(17), 2557. https://doi.org/10.3390/foods11172557

Porras-Saavedra, J., Pérez-Pérez, N. C., Villalobos-Castillejos, F., Alamilla-Beltrán, L., & Tovar-Benítez, T. (2021). Influence of Sechium edule starch on the physical and chemical properties of multicomponent microcapsules obtained by spray-drying. *Food Bioscience*. https://doi.org/10.1016/j.fbio.2021.101275

Premjit, Y., Pandhi, S., Kumar, A., Rai, D. C., Duary, R. K., & Mahato, D. K. (2022). Current trends in flavor encapsulation: A comprehensive review of emerging encapsulation techniques, flavour release, and mathematical modelling. *In Food Research International*. https://doi.org/10.1016/j.foodres.2021.110879

Rezaei, N., Mehrnejad, F., Vaezi, Z., Sedghi, M., Asghari, S. M., & Naderi-Manesh, H. (2020). Encapsulation of an endostatin peptide in liposomes: Stability, release, and cytotoxicity study. *Colloids and Surfaces B: Biointerfaces.*. https://doi.org/10.1016/j.colsurfb.2019.110552

Rizkyana, A. D., Ho, T. C., Roy, V. C., Park, J.-S., Kiddane, A. T., Kim, G.-D., & Chun, B.-S. (2022). Sulfation and characterization of polysaccharides from Oyster mushroom (Pleurotus ostreatus) extracted using subcritical water. *The Journal of Supercritical Fluids, 179*, Article 105412. https://doi.org/10.1016/j.supflu.2021.105412

Sabet, S., Rashidinejad, A., Melton, L. D., Zujovic, Z., Akbarinejad, A., Nieuwoudt, M., Seal, C. K., & McGillivray, D. J. (2021). The interactions between the two negatively charged polysaccharides: Gum Arabic and alginate. *Food Hydrocolloids, 112*, Article 106343. https://doi.org/10.1016/j.foodhyd.2020.106343

Santos, P. D. de F., Batista, P. S., Torres, L. C. R., Thomazini, M., de Alencar, S. M., & Favaro-Trindade, C. S. (2023). Application of spray drying, spray chilling and the

combination of both methods to produce tucumã oil microparticles: characterization, stability, and β-carotene bioaccessibility. *Food Research International*, *172*, 113174. https://doi.org/10.1016/j.foodres.2023.113174.

Shrotri, A., Kobayashi, H., & Fukuoka, A. (2017). *Catalytic Conversion of Structural Carbohydrates and Lignin to Chemicals* (pp. 59–123). https://doi.org/10.1016/bs.acat.2017.09.002.

Silva Faria, W. C., da Conceição, E. C., Moura, W. de M., Barros, W. M. de, Converti, A., & Bragagnolo, N. (2020). Design and evaluation of microencapsulated systems containing extract of whole green coffee fruit rich in phenolic acids. *Food Hydrocolloids*. https://doi.org/10.1016/j.foodhyd.2019.105437.

Teixeira, L. S., Martim, S. R., Silva, L. S. C., Kinupp, V. F., Teixeira, M. F. S., & Porto, A. L. F. (2016). Efficiency of Amazonian tubers flours in modulating gut microbiota of male rats. *Innovative Food Science and Emerging Technologies*. https://doi.org/10.1016/j.ifset.2016.08.015

Truzzi, E., Marchetti, L., Benvenuti, S., Ferroni, A., Rossi, M. C., & Bertelli, D. (2021). Novel Strategy for the Recognition of Adulterant Vegetable Oils in Essential Oils Commonly Used in Food Industries by Applying 13C NMR Spectroscopy. *Journal of Agricultural and Food Chemistry*. https://doi.org/10.1021/acs.jafc.1c02279

Tzatsi, P., & Goula, A. M. (2021). Encapsulation of Extract from Unused Chokeberries by Spray Drying, Co-crystallization, and Ionic Gelation. *Waste and Biomass Valorization, 12*(8), 4567–4585. https://doi.org/10.1007/s12649-020-01316-7

Ugwu, C. E., Kenechukwu, F. C., Diovu, E. O., Udodeme, H. O., Momoh, M. A., Onuigbo, E. B., & Attama, A. A. (2022). Exploitation of capsule system for colon targeted drug delivery of biopolymer-based microparticles: In vivo and in vitro applications. *Heliyon*. https://doi.org/10.1016/j.heliyon.2022.e11390

Wang, L., Wei, Z., Xue, C., & Yang, L. (2023). Co-delivery system based on multilayer structural nanoparticles for programmed sequential release of fucoxanthin and curcumin. *Food Hydrocolloids, 141*, Article 108729. https://doi.org/10.1016/j.foodhyd.2023.108729

Zhang, L., Ueno, S., Miura, S., & Sato, K. (2007). Binary Phase Behavior of 1,3-Dipalmitoyl-2-oleoyl-sn-glycerol and 1,2-Dioleoyl-3-palmitoyl-rac-glycerol. *Journal of the American Oil Chemists' Society, 84*(3), 219–227. https://doi.org/10.1007/s11746-006-1034-0